Preferential Crystallization: Multi-Objective Optimization Framework

Shrikant A. Bhat and Biao Huang
Dept. of Chemical and Materials Engineering, University of Alberta, Edmonton, Alberta, Canada

DOI 10.1002/aic.11691
Published online January 2, 2009 in Wiley InterScience (www.interscience.wiley.com).

A four objective optimization framework for preferential crystallization of D-L threonine solution is presented. The objectives are maximization of average crystal size and productivity, and minimization of batch time and the coefficient of variation at the desired purity while respecting design and operating constraints. The cooling rate, enantiomeric excess of the preferred enantiomer, and the mass of seeds are used as the decision variables. The optimization problem is solved by using adaptation of the nondominated sorting genetic algorithm. The results obtained clearly distinguish different regimes of interest during preferential crystallization. The multi-objective analysis presented in this study is generic and gives a simplified picture in terms of three zones of operations obtained because of relative importance of nucleation and growth. Such analysis is of great importance in providing better insight for design and decision making, and improving the performance of the preferential crystallization that is considered as a promising future alternative to chromatographic separation of enantiomers.
 AIChE J, 55: 383–395, 2009
Keywords: preferential crystallization, enantiomers, genetic algorithm, multi-objective optimization

Introduction

Enantiomers or chiral compounds are the stereoisomers that are nonsuper imposable, but are mirror images of each other. The important property of enantiomers is that they rotate the plane-polarized light by equal amounts, but in opposite directions. Depending on the direction of rotation of the plane polarized light, they are distinguished as "+" or "−" or "D" or "L" type. Although the chiral compounds usually have similar chemical and physical properties, they differ in metabolic activities.[1] Molecular chirality is of importance through its application to stereochemistry in inorganic, organic, and physical chemistry as well as biochemistry and supramolecular chemistry. One of the important applications of enantiomers is as a drug in pharmaceutical industries. The manufacturing of enantiomers usually gives products in the form of mixture of equal percentage of both the enantiomers called racemic mixture or racemates. In many cases, the drugs can be administered as racemates with only one of the enantiomers active. However, recent trends in drug discovery have been toward development of one type of enantiomer as there are cases in which the counter enantiomer may have a harmful effect on the metabolic activity.[2] Thus, selective production of enantiomers or separation of the preferred enantiomer from racemates are two attractive propositions.

Preferential crystallization involving selective crystallization of the preferred enantiomer has economical advantages over various manufacturing processes producing the selected enantiomer[1] or the existing chromatographic separation processes,[3,4] and has a potential as the most viable future alternative. This is a technique applied to the mixture of enantiomers belonging to the class of conglomerates, that is, the physical mixtures of crystals where each crystal is pure enatiometrically and has a distinct structural identity. Extensive work in both the experimental and theoretical aspects in

Correspondence concerning this article should be addressed to B. Huang at biao.huang@ualberta.ca.

the field of preferential crystallization has been reported by Seidel-Morgenstern, Elsner and coworkers.[5–10] The contribution is mainly in terms of detailed high resolution as well as moment based models for preferential crystallization; evaluation of the rate constants for growth and nucleation, and studies related to single objective optimization and various intensification strategies. The experimental insights obtained are very helpful in model building and validation of various optimization and control strategies.

In general, the optimization objectives for crystallization are to maximize the mean crystal size, minimize the coefficient of variation, the batch time, and the ratio of mass of crystals formed by nucleation to that by seeding, etc. Because of the inherent relation between nucleation and growth of a crystal to the extent of supersaturation, the optimum supersaturation has to be such that the desired objectives are achieved while respecting design and operating constraints. Although there are many studies that manipulate only the temperature profile to get the optimum product properties,[11–15] there are many other experimental as well as simulation approaches that use seed amount and size as an additional variable to manipulate product properties.[16–21] This gives an additional degree of freedom in attaining the optimal configuration. Most of these studies, however, deal with single objectives and those involving multi-objective optimization use a single objective optimization coupling one or more important objectives into a single one.[17,22,23] For example, the objective of the maximum crystal size and minimum coefficient of variation has been solved by taking the weighted ratio of the two as a single objective,[22,23] and the problem of minimization of the batch time while achieving the maximum crystal size has been solved by maximizing the size while using a penalty for the batch time.[17] Such solution approaches hide the physical significance of various objectives and the solution of the problem depends on the weights assigned to different objectives. It may not also be possible to judiciously assign weights to different objectives as it is difficult and unrealistic to relate two or more objectives of different nature. For crystallization, different temperature profiles and the amount of seeds impose complex interplay between various desired objectives and can be addressed effectively only by considering all the objectives simultaneously but distinctively in a multiobjective optimization framework.

Genetic algorithm and its adaptations have evolved as efficient approaches for multi-objective optimization for most of the areas in science and engineering. Originally proposed by Goldberg[24] as a simple genetic algorithm (SGA) for the single objective optimization, the genetic algorithm is based on the principle of evolution, that is, the survival of the fittest strategy, to find the optimal solution. Because of the distributed population based approaches and the nature of progression, this algorithm tends to reach the global optimum. Adaptation of the genetic algorithm to handle multiple objectives involves considering simultaneously all the objectives and derives a set of nondominating solutions called Pareto optimal solutions. All the solutions in the Pareto set are optimal with respect to one or more objectives and they give a comprehensive picture to the decision maker to choose an appropriate solution based on his/her requirements. Amongst various multi-objective adaptations of the genetic algorithm, the nondominated sorting genetic algorithm (NSGA-II)[25] has been widely used in many areas in engineering optimization. A significant contribution in the area of the multi-objective optimization in the field of chemical engineering is due to Gupta and coworkers[26] through various adaptation of NSGA-II to different complex systems such as the polymerization reactor, fluidized bed catalytic cracker,[27] membrane separation,[28] heat integration,[29] etc. As far as multi-objective optimization in crystallization is concerned, the first and the latest effort has been by Sarkar et al.[30] for optimization of seeded batch cooling crystallization using NSGA-II for problems involving two and three objectives. Amanullah and Mazzotti[31] have also reported a genetic-algorithm-based two-objective optimization for hybrid chromatography-crystallization process for the separation of Troger's base enantiomers. They however considered a simple mass balance approach for modeling the crystallization process. The multi-objective optimization in the field of preferential crystallization has not been attempted yet although studies related to the single objective optimization have recently been reported.[32]

This study analyses the preferential crystallization from the multi-objective optimization point of view by considering four objectives simultaneously. The system under consideration is the batch-wise preferential crystallization of D-L threonine solution previously considered by Angelov et al.[32] for a single objective optimization. The same work is extended here to a more comprehensive multi-objective framework with more decision variables, thus, enabling additional degree of freedom and providing more comprehensive picture. As a result of multi-objective optimization new phenomena in terms of formation of three optimal regions of interest in the four-objective search space are observed, and analyzed in detail in this work. These regions are formed because of relative change in the domination of various events such as nucleation, nuclei growth, initial seed distribution, and seed growth during the entire crystallization regime. Such qualitative as well as quantitative evaluation has not been reported earlier in the literature. The analysis presented in this study is generic and applies equally to other similar crystallizing systems. The remainder of this article is organized as follows. The modeling framework for preferential crystallization is presented in the second section. The multi-objective optimization problem formulation and operating constraints are illustrated in the third section. The fourth section briefly describes the genetic algorithm framework employed to solve this problem. The fifth section presents the results and discussion, followed by conclusions in the last section.

Preferential Crystallization: Modeling

In preferential crystallization, the preferred p-enantiomer is selectively separated from the solution containing mixture of both p-enantiomer and the counter, c-enantiomer (with equal or unequal proportion). If supersaturation is maintained in the metastable regime (the zone where no spontaneous primary nucleation takes place) with seeding of the p-enantiomer, then the p-form will be preferably crystallized. The

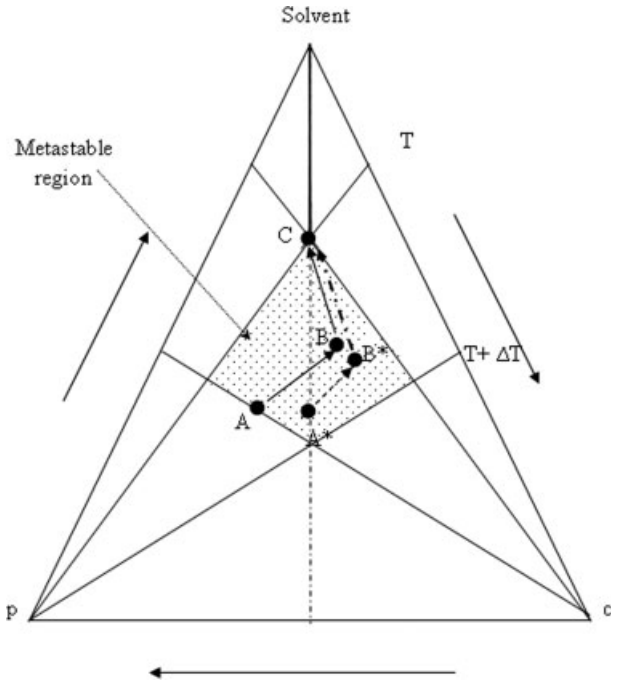

Figure 1. Principle of preferential crystallization.

separation is based on the different crystal surface areas of both the enantiomers that have been provided initially. This can be illustrated better from the ternary diagram[32] in Figure 1. The three vertices indicated by solvent, p and c denote pure solvent, p-form and c-form, respectively. The shaded region between the temperature ranges T and $T + \Delta T$ is the metastable region. If we start at the point A, seed the solution with crystals of p form and reduce temperature to T, selective crystallization of p form will take place and the concentration of the solution will move along path AB. However, it has been observed experimentally[32] that after some time spontaneous crystallization of c-form starts and eventually the solution is brought to the equilibrium point C. It is therefore important that the operation is stopped around point B to get the pure p-form. In this case, we have considered enantiomeric excess with respect to p-form (Point A), that is, solution at point A is richer in p-form when compared to c-form. Enantiomeric excess is considered beneficial for the separation process, but is not strictly necessary. We can start from point A* as well, which represents equal proportion of both the enantiomeric forms. Now, if we seed the solution with p form, the trajectory A*-B*-C will be followed. The crystallization can be stopped at point B* to selectively separate the p-form crystals. Detailed description of this phenomena can be found in the study reported by Elsner et al.[33] To obtain the desired purity of the p-form, we should try to assess the effect of the temperature profile, enantiomeric excess, seed size, and distribution on the purity and productivity of the desired enantiomers. This can be addressed by the population balance based modeling framework which is briefly described below.

Consider a well mixed batch crystallizer with the solution of both the enantiomers at temperature T. We assume that there is no agglomeration, breakage and dissolution, and $G_{(s)}$ and $B_{(s)}$ represent the effective growth and nucleation rate for the enantiomers $s \in (p,c)$. $G_{(s)}$ has also been assumed to be size independent. Under these assumptions, the resulting population balance equation[34] is of the following form:

$$\frac{\partial N_{(s)}(t,x)}{\partial t} = -G_{(s)} \frac{\partial}{\partial x}\left(N_{(s)}(t,x)\right), \quad s \in (p, c) \tag{1}$$

The boundary and initial conditions for this equation are as follows

$$N_{(s)}(t,0) = \frac{B_{(s)}}{G_{(s)}}, \quad s \in (p,c) \tag{2}$$

$$N_{(p)}(0,x) = N_{(p,\text{seed})}(x) \tag{3}$$

$$N_{(c)}(0,x) = 0 \tag{4}$$

where, $N_{(s)}(t,x)$ denotes the number density of the particles of size x at time t and $N_{(p,\text{seed})}(x)$ denotes the number density of seeds of the p form of size x. Eq. 1 represents the rate of evolution of number density of the particles of size x with time.

As far as crystal growth is concerned, there are many mechanisms that take place simultaneously which contribute to this. It is difficult to accommodate all the mechanisms in a population balance framework and the model becomes very complex as the evaluation of various parameters associated with this complex model is very difficult task. However, a simple power law expression gives a good approximation and has been used widely.[30,32,35] In this study, we use the growth rate model proposed by Angelov et al.[32] This model describes the growth rate as a function of supersaturation as follows:

$$G_{(s)} = k_{G,\text{eff}}(\text{Su}_{(s)} - 1)^{\text{gr}} \tag{5}$$

$$\text{Su}_{(s)} = \frac{m_{(s)}}{m_{(\text{eq},s)}} \tag{6}$$

$$m_{(p)} = \frac{M_{\text{p,liq}}}{M_{\text{p,liq}} + M_{\text{c,liq}} + M_{\text{w}}} \tag{7}$$

$$m_{(c)} = \frac{M_{c,\text{liq}}}{M_{p,\text{liq}} + M_{c,\text{liq}} + M_{\text{w}}} \tag{8}$$

$$m_{(\text{eq},p)} = \sum_{k=0}^{2} a_{p,k}T^k + m_c \sum_{k=0}^{2} b_{p,k}T^k \tag{9}$$

$$m_{(\text{eq},c)} = \sum_{k=0}^{2} a_{c,k}\text{T}^k + m_p \sum_{k=0}^{2} b_{c,k}T^k \tag{10}$$

where, $k_{G,\text{eff}}$ is the effective growth rate, $\text{Su}_{(s)}$ represents the extent of supersaturation, and gr is the growth exponent. $\text{Su}_{(s)}$ is determined as the ratio of the mass fraction, $m_{(s)}$, of enantiomer s to its equivalent mass fraction, $m_{(\text{eq},s)}$, determined as the function of temperature, T, and the mass fraction of the other enantiomer. $M_{\text{liq},s}$ is the mass of the enantiomer s dissolved in water and M_w is the mass of water. $a_{s,k}$ and $b_{s,k}$ $s \in (p,c)$ are empirical constants.

The rate of nucleation for both the enantiomers is given as a function of supersaturation by[36]

$$B_p = k_{b,p,\text{eff}}\left(\text{Su}_{(p)} - 1\right)^{bp}\mu_3^p(t) \tag{11}$$

$$B_c = k_{b,c,\text{eff}}e^{-bc/\ln^2 \text{Su}_{(c)}} \tag{12}$$

where, $k_{b,p,\text{eff}}$ and $k_{b,c,\text{eff}}$ are the effective nucleation rate constants for p and c forms, bp and bc are exponential coefficients, and μ_3^p is the third moment for the p-form.

Angelov et al.[32] used the Arrhenius approach to establish dependence of $k_{G,\text{eff}}$ and $k_{b,p,\text{eff}}$ on T and the angular rate of impeller, w as follows:

$$k_{G,\text{eff}} = k_{G,\text{eff},0}\exp\left(\frac{-E_G}{R(T+273.15)}\right) \tag{13}$$

$$k_{G,\text{eff},0} = k_{G,0}w^{\text{ng}} \tag{14}$$

$$k_{b,p,\text{eff}} = k_{b,p,\text{eff},0}\exp\left(\frac{-E_{bp}}{R(T+273.15)}\right) \tag{15}$$

$$k_{b,p,\text{eff},0} = k_{b,p,0}\exp\left(\frac{nb}{w}\right) \tag{16}$$

where, E_G and E_{bp} are the energy parameters associated with growth and nucleation, and nb, ng, $k_{G,0}$, and $k_{b,p,0}$ are the empirical parameters obtained from experimental data.[32]

To solve these population balance equations we also need to include the material balance of both the enantiomers to evaluate the extent of super saturation which governs the growth and nucleation rate of both the enantiomers. The mass balance for enantiomer s in general is given by

$$\frac{dM_{(liq,s)}(t)}{dt} = -3\rho k_v G_{(s)}\int_0^\infty \left(N_{(s)}(t,x)\right)x^2dx, \quad s \in (p,\ c) \tag{17}$$

The population balance model Eqs. 1–4 can be solved by numerical discretization in the x domain to convert the partial differential equations (PDEs) into ordinary differential equations (ODEs). The resulting set of ODEs can be solved along with Eq. 17 to evaluate the particle size evolution with time. Various high resolution methods have been proposed in the literature to solve the population balance equations and comparative evaluation of these numerical schemes, specifically for preferential crystallization, has been attempted by Qamar et al.,[9] focusing on various aspects such as numerical diffusion, accuracy and computational time. However, the most widely used method for solving the population balance equation for use in optimization and control is a scheme based on the first few moments of the crystal size distribution[32,35] although there are a few studies involving use of a high resolution models for optimization.[15,30] The scheme based on moments is, however, faster, gives fairly good representation of the process, and is used in this study. In fact, Angelov et al.[32] have used the moment based model for optimization of the same preferential crystallization system in their latest single objective optimization framework and this study is the extension of their work to a more comprehensive four objective optimization framework. Once the overall insights are obtained, detailed models can be used for optimization in the region of interest to further refine the results (not reported in this study). Therefore, we use the moment based model in this study for the multi-objective optimization.

The model based on moments as proposed by Randolph and Larson[37] gives the following set of ODEs for the population balance Eqs. 1–4.

$$\frac{d\mu_{s,0}}{dt} = B_s \tag{18}$$

$$\frac{d\mu_{s,i}}{dt} = iG_{(s)}\mu_{s,i-1} \quad i = 1,2,\ldots \tag{19}$$

where, $\mu_{s,i}$ is the i^{th} moment of s form defined as

$$\mu_{s,i} = \int_0^\infty x^i N_s(t,x)dx \tag{20}$$

In general, the first four moments give reasonably good approximation for the crystal size distribution and the ODEs corresponding to these four sets of moments are solved along with the Eq. 17 to arrive at the crystal size distribution as a function of time.

Some important properties of crystal size distribution obtained from the moments are:

$$\text{Average crystal size, } S_{\text{avg}} = \frac{\mu_1}{\mu_0} \tag{21}$$

$$\text{Coefficient of variation, CV} = \sqrt{\left(\frac{\mu_2\mu_0}{\mu_1^2} - 1\right)} \tag{22}$$

There are various other ratios that can be used to calculate S_{avg} and CV based on the other moments. In this study, we use the definitions stated above.

Multi-Objective Optimization Framework

The important objectives for batch preferential crystallizers are minimization of batch time, tf, and the coefficient of variation, CV while maximizing S_{avg} and productivity, Pr, for the desired purity, Pu_{des}. The decision variables are the mass of seed of the preferred enantiomer, Ms, temperature history, $T(t)$, batch time, tf, and initial enantiomeric excess, ee. The constraints involve model constraints, the allowable range of rate of cooling, Q, the desired purity, Pu_{des}, of the p-form, and the temperature range of operation to ensure crystallization within the metastable zone.

The initial enantiomer excess, ee, is defined as,

$$\text{ee} = \left.\frac{M_{p,\text{liq}} - M_{c,\text{liq}}}{M_{p,\text{liq}} + M_{c,\text{liq}}}\right|_{t=0} \tag{23}$$

The productivity is defined as,

$$Pr = \frac{\text{Total mass of p} - \text{form crystals produced at time tf} - M_s - \text{ee}(\text{M}_{p,\text{liq}} + M_{c,\text{liq}})_{t=0}}{\text{Mass of enantiomer in racemate} - \text{ee}(M_{p,\text{liq}} + M_{c,\text{liq}})_{t=0}} \tag{24}$$

Table 1. Values of Parameters used in Model Eqs. 17–19 and 24

Parameters	Value	Unit	Parameters	Value	Unit
$a_{0,c}$	5.7405×10^{-2}	–	T_{min}	25	°C
$a_{1,c}$	1.3584×10^{-3}	1/°C	T_{max}	34	°C
$a_{2,c}$	-2.3638×10^{-6}	1/°C^2	$Pu_{desired}$	0.95	–
$a_{0,p}$	5.615×10^{-2}	–	ee_{min}	0	%
$a_{1,p}$	1.4384×10^{-3}	1/°C	ee_{max}	6	%
$a_{2,p}$	-3.4178×10^{-6}	1/°C^2	Ms_{min}	0	kg
$b_{0,c}$	7.1391×10^{-3}	–	Ms_{max}	10×10^{-3}	kg
$b_{1,c}$	-3.8367×10^{-3}	1/°C	tf_{max}	400	min
$b_{2,c}$	4.2345×10^{-5}	1/°C^2	T_{init}	32–34	°C
$b_{0,p}$	6.2444×10^{-3}	–	Q_{max}	−0.2	°C/min
$b_{1,p}$	-3.9185×10^{-3}	1/°C	Pr_{min}	0.005	–
$b_{2,p}$	4.4174×10^{-5}	1/°C^2	M_w	$1- M_{c,liq}- M_{p,liq}$	kg
bp	4	–	$M_{c,liq}$	0.100224	kg
bc	6×10^{-2}	–	W	2000	min^{-1}
E_g	75.6×10^3	J/mol	N_{pop}	400	–
E_{bp}	78.7×10^3	J/mol	p_c	0.9	–
R	8.3145×10^3	J/mol	p_m	0.0033	–
Gr	1	–	L_c	660	–
$k_{b,c,eff}$	3.84×10^6	1/min	L_s	30	–
$k_{b,p,0}$	5.788×10^{16}	1/(mm.min)			
$k_{g,0}$	1.1375×10^{10}	mm min$^{-0.54}$			
k_v	2.48×10^{-2}	–			
ρ	1.25×10^{-6}	kg/mm^3			
ng	0.46	–			
nb	1.8228×10^3	1/min			

The productivity is defined in such a way that this gives the fraction of the net p-form produced from the racemic mixture assuming that only the racemic mixture is available to start with. The numerator gives the mass of the crystal formed over and above the mass of seed and the p-form used to achieve the desired ee. The denominator gives the total mass of racemic mixture before addition of p-form crystals to achieve desired ee. The initial seed size distribution for p form is assumed to be[38]

$$N_{(p)}(x,0) = \frac{1}{\sqrt{2\pi}\sigma K}\frac{1}{x}\exp\left[-\frac{1}{2}\left(\frac{\ln x - \theta}{\sigma}\right)^2\right] \tag{25a}$$

$$K = \frac{k_v \rho_s}{Ms}\mu_3^p(t=0) \tag{25b}$$

where, $\sigma = 0.3947$ and $\theta = -6.8263$ are determined from experiments,[38] and the initial moments are determined using Eq. 20. The discretization is done for the maximum length of 5 mm with an interval of 0.05 mm to calculate the initial moments.

In this work, we consider the following four-objective optimization problem involving temperature profile, T(t), Ms, ee and tf as decision variables.

$$\begin{aligned}
&\text{Max } S_{avg}\\
&\text{Max Pr}\\
&\text{Min CV}\\
&\text{Min tf}\\
&\text{Decision variable: } M_s;\ T(t);\ \text{tf};\ \text{ee}\\
&\text{Subject to:}\\
&\text{Model constraints: Eqs 17–19}\\
&0 \le Q \le Q_{max}\\
&T_{min} \le T(t) \le T_{max}\\
&Pu(tf) = Pu_{desired}\\
&ee_{min} \le ee \le ee_{max}\\
&Ms_{min} \le Ms \le Ms_{max}\\
&0 \le tf \le tf_{max}
\end{aligned} \tag{26}$$

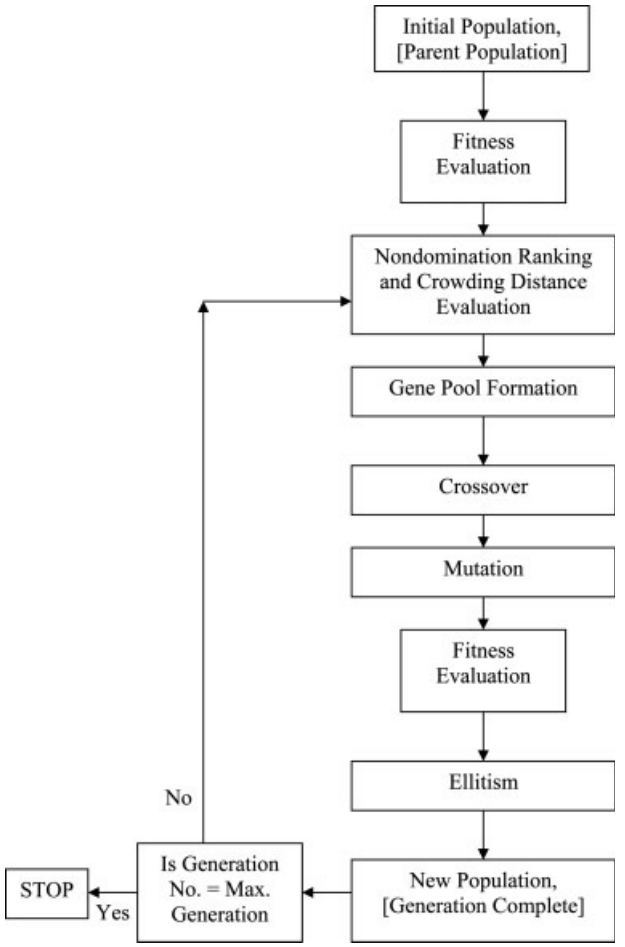

Figure 2. Flowchart for nondominated sorting genetic algorithm.

Table 2. Reference Conditions for Sensitivity Analysis

Mass of Seed, M_s (kg)	Enantiomeric Excess, ee (%)	Rate of Cooling (°C/min)
5×10^{-3}	3	0.05

The above problem is solved using nondominated sorting genetic algorithm II (NSGA-II) originally proposed by Deb et al.[25] NSGA-II deals with discrete decision variables. To use the continuous temperature history, $T(t)$ is descretized into 20 discrete values, T_1 to T_{20}, within the time interval of 400 min. The temperature values between each discrete interval are obtained by using Hermite interpolation.[39] To take into account the constraint on the cooling rate, Q (the rate at which the solution is cooled), the successive values from T_1 to T_2 are selected so as to be within the acceptable cooling rate. The model equations are solved using the Gear's Package from NAG Fortran Library (D02EJF). The integration is terminated as the desired purity is obtained. This handles the purity constraint for all the solutions that are produced during successive generations. The values of all the four objectives at this time are considered for the given sets of decision variables. This procedure coincides with the similar study on optimization of bulk polymerization of methyl methacrylate in a batch reactor.[40] In this study, $T(t)$ was used as a decision variable to minimize batch time to obtain desired end product properties.

For the four-objective optimization problem, because Pr is defined as the net mass of the crystals produced over and above the excess enantiomer added and the mass of the seed, we are likely to get solutions where the mass of crystal obtained is less than amount of the excess enantiomer used. This will give rise to negative Pr and is considered undesired. Also for practical requirements, it is important to explore the regime where Pr is more than certain minimum desired limit. This is achieved by penalty function method, that is, destroying the solutions corresponding to Pr less than the desired minimum value, Pr_{min}, by assigning less objective function values (-1×10^{-10}) corresponding to these solutions. The values of the parameters used in the model Eqs. 17–19 and 26 are taken from Angelov et al.[32] and Elsner et al.,[33] and are given in Table 1.

Genetic Algorithm Framework

In this section, we present a brief description of nondominated sorting genetic algorithm for the sake of completeness.

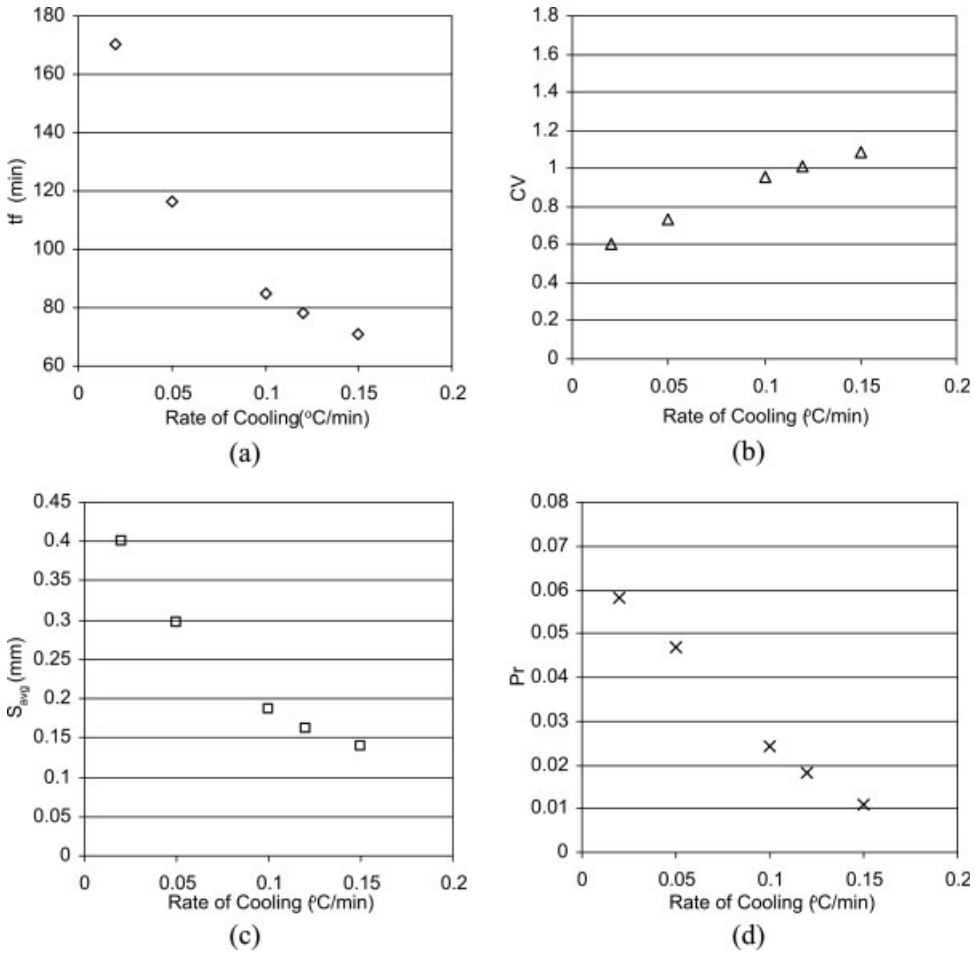

Figure 3. Effect of cooling rate on (a) tf, (b) CV, (c) S_{avg}, and (d) Pr.

This algorithm is discussed in much detail by Deb et al.[25] Genetic algorithm is a search-based evolutionary optimization technique inspired from the Darwin's principle of survival of the fittest. This involves assigning bounds for decision variables, their mapping in the binary/real domain as chromosomes, and subsequent operations of reproduction in terms of crossover and mutation in a stochastic way followed by elitism. The important parameters associated with the genetic algorithm are the initial population size (the number of initial solutions), N_{pop}, the probability of crossover, p_c, and mutation, p_m, length of chromosome, L_c, length of the string, L_s, corresponding to each decision variable and the upper and lower bounds on decision variables.

The initial population is randomly generated. For single objective optimization the objective function corresponds to the fitness of the member of the population. On the basis of the fitness of the individuals, a gene pool is formed where each member of the population is introduced based on the probability proportional to its relative fitness with respect to the rest of the members. Thus, gene pool has more contribution from the fitter individuals. This is followed by random crossover and mutation amongst the members of the gene pool to produce new population. Fitness of all the new population members are compared with the original population members and only the first best N_{pop} individuals are retained for the next generation (elitism). In case of multiobjective optimization, the members of the population are categorized based on their nondomination and crowding distance and fitness is assigned to them based on their rank of nondomination and the spread corresponding to their neighboring solutions. This is followed by the formation of gene pool, crossover, mutation and elitism. Figure 2 gives a flow chart for this algorithm.

One of the important aspects in this study is the way crossover is implemented. Between any two members from the gene pool selected for crossover, only the length of the chromosome which covers temperature values till tf (for both chromosomes) is important. Therefore, crossover is randomly done at those sites in a chromosome which represent string corresponding to the time which is minimum of the two tf values corresponding to the two chromosomes that are considered.

There are various adaptations of the genetic algorithm aimed to accelerate convergence to the global optimization based on the concept of jumping gene.[27,28] These algorithms are only slightly better (or as good) in arriving at the solutions for the problem discussed in this study. The nature of the Pareto optimal region remains almost the same for all different adaptations. As the main focus of this study is to analyze various scenarios arising due to multi-objective

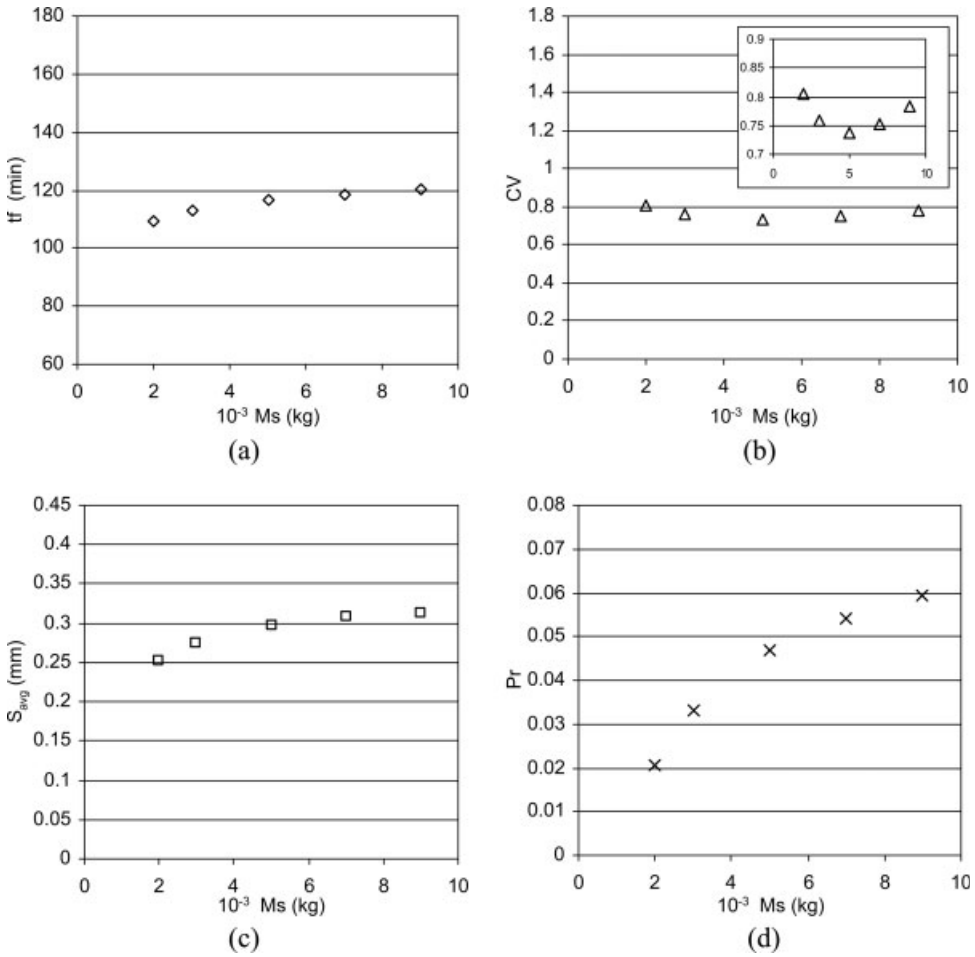

Figure 4. Effect of Ms on (a) tf, (b) CV, (c) S_{avg}, and (d) Pr.

analysis, only the basic genetic algorithm framework (NSGA-II) is considered. Some new adaptations to the genetic algorithm framework to get significant acceleration in the genetic algorithm and their comparison *vis a vis* the basic NSGA-II algorithm and jumping gene adaptations is being attempted and would appear in forthcoming publications.

Results and Discussion

We first analyze the effect of the decision variables on the objective functions. Table 2 shows the reference conditions based on which the sensitivity analysis was performed. One of the variables is changed while keeping the other two fixed at the values given in Table 2 and its effect on the values of objective functions is observed. Figures 3–5 show the effect of change in cooling rate, Ms and ee, on the S_{avg}, tf, CV and Pr at desired purity of 95% of the p-form.

The increased rate of cooling decreases the time required to get the desired purity of the product, but at the expense of decreased Pr and S_{avg} and increased CV. This occurs as primary nucleation is favored for both the p and c form as the rate of cooling is increased, thus reducing Pr and S_{avg} and increasing CV. Increased Ms increases Pr and S_{avg} but increases tf as well. This is because seed growth is favored as mass of seeds is increased and nucleation for both the p and c form is suppressed. Reduced nucleation of c-form promotes more growth of p-form and will require longer time to attain desired purity, but this will also result in increased productivity. The effect of Ms on CV shows CV going through a minimum. This is due to relative change in nucleation and seed growth (or initial seed distribution) achieved with the change in the mass of seed. This will be explained in detail toward the end of this section. Increase in ee does not have significant effect on tf, although there is slight reduction as seen in Figure 5a. This, however, favors reduced CV while increasing S_{avg} and Pr due to favorable nucleation of the p-form. The analysis presented here is not comprehensive, but it clearly highlights the fact that the effect of the decision variables on the objective functions is in different directions and to varying extents. Hence, the combined effect of all the decision variables on the four objectives would be complex and there is a need to explore this within the multi-objective optimization framework.

Figure 6 shows the Pareto optimal solution for the four-objective optimization problem described in Eq. 26. This is the solution obtained at the 10,000th generation. No further improvement in the Pareto solution is obtained beyond this point. The values of the various parameters used in the genetic algorithm are given in Table 1. All the four objectives are plotted on six two-dimensional plots as shown in

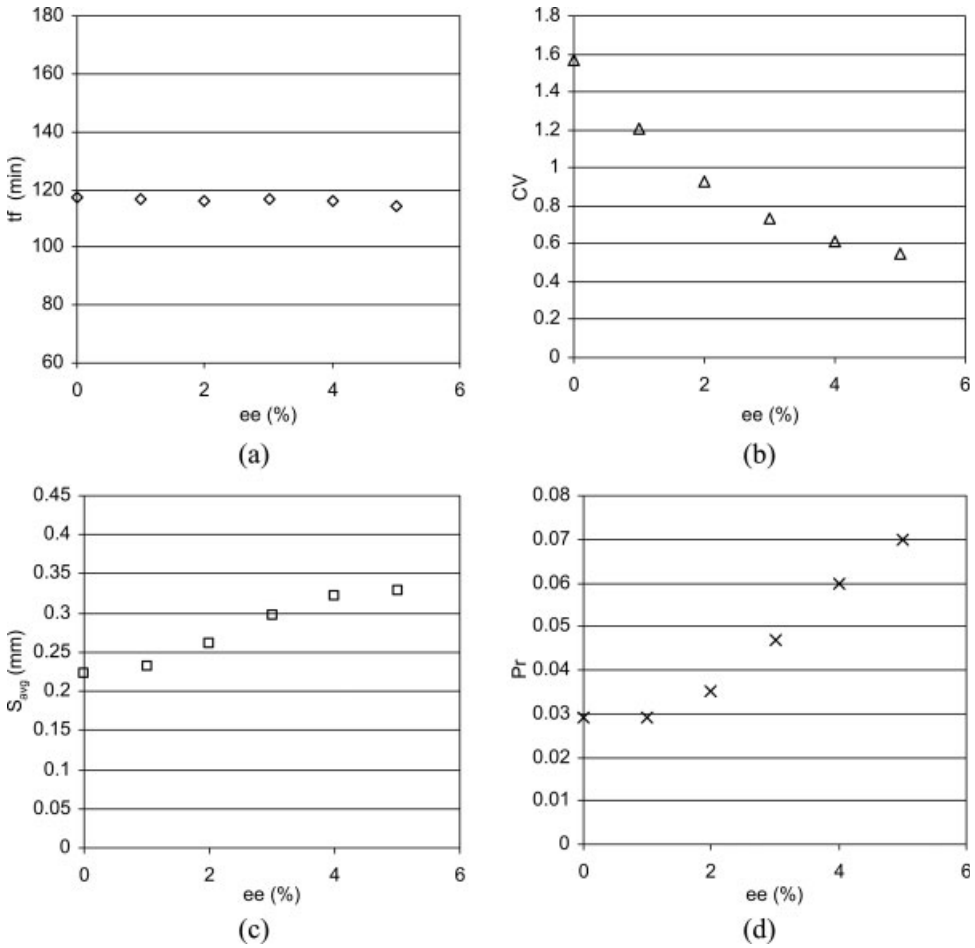

Figure 5. Effect of ee on (a) tf, (b) CV, (c) S_{avg}, and (d) Pr.

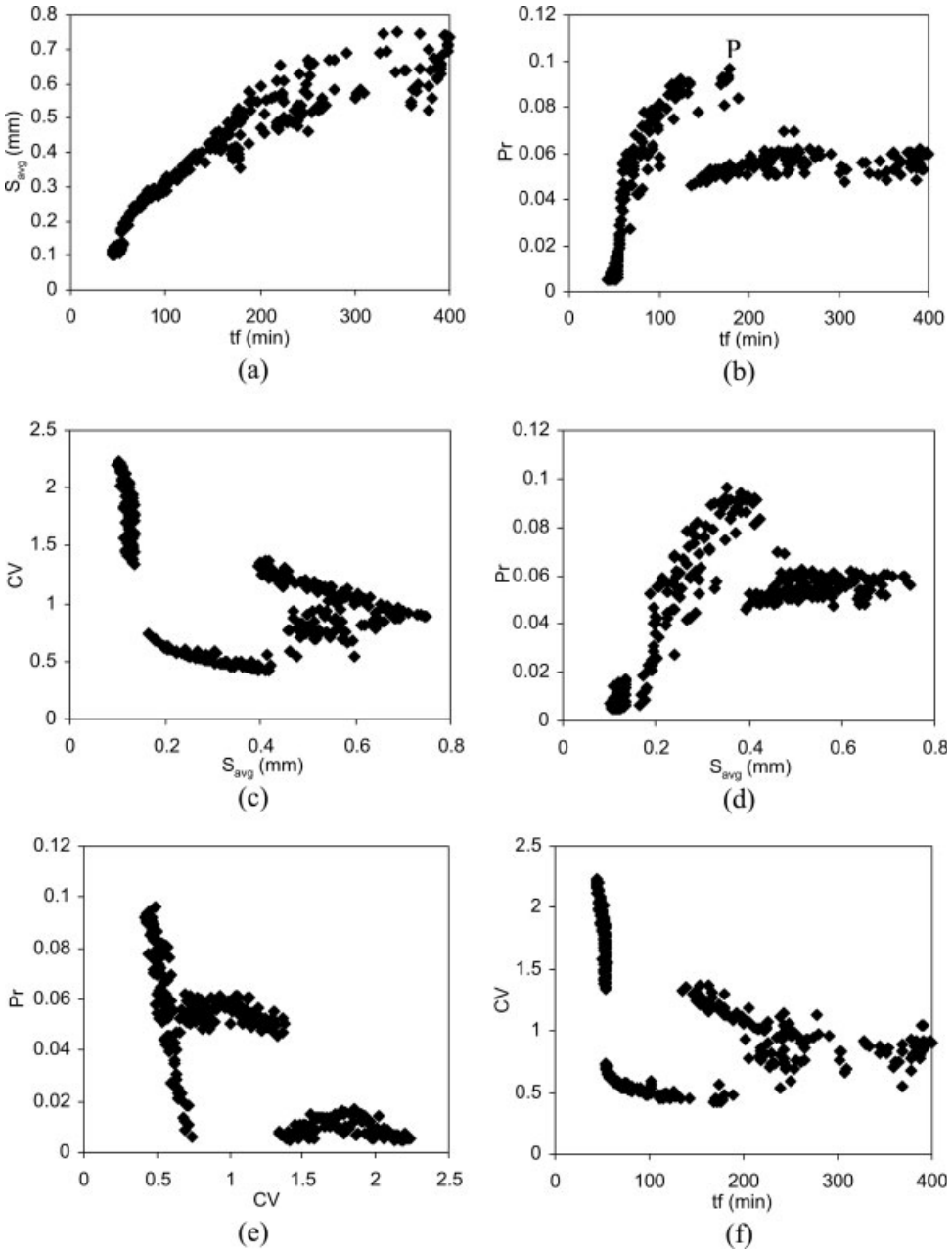

Figure 6. Pareto optimal solution for the four objective optimization problem (Eq. 26).

Figure 6. All the solutions in the figures are nondominating, that is, all of them are better in one or more objectives than the rest of them. The optimal average crystal size (p-form) almost monotonically increases with tf (Figure 6a) for lower values of tf followed by increase in the spread for higher tf values. However, there is a maximum in the Pr observed with respect to tf and S_{avg} at the given purity (Figures 6b, d). CV decreases with increase in average size and tf, followed by a further increase (Figures 6c, f). There are three distinct regions observed in the CV vs. S_{avg} as well as CV vs. tf plots (Figures 6c, f and Figure 7). This is due to relative significance of primary nucleation and nuclei/seed growth during the entire crystallization regime. It can be assessed by analyzing particle size distribution using the detailed population balance model. To assess this, the length of the crystal is considered from 0 to 5 mm with discretization interval of 0.05 mm and the initial seed size distribution is obtained using Eq. 25.

We now present the detailed particle size distribution at the eight points A–H indicated in Figure 7 for further illustration. Figures 8a, b show the crystal size distribution due to primary nucleation and subsequent growth of the nuclei, and the distribution due to seed growth for the p-form, respectively, for the points A-G of Figure 7 (note the change of scale in Y-axis for these figures). Figure 8c shows the crystal size distribution due to primary nucleation and subsequent growth of these nuclei for the c-form. Table 3 shows the operating conditions for these points. For two points in Zone 1

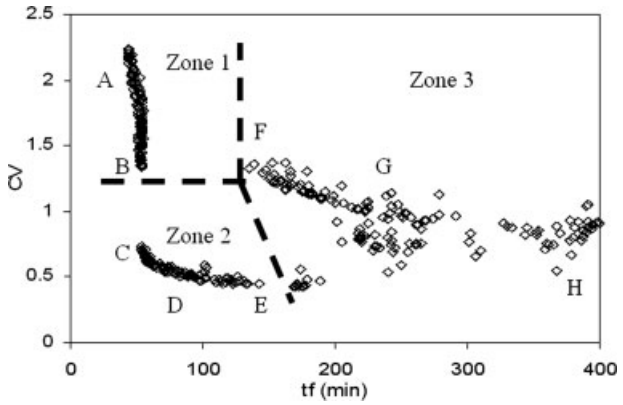

Figure 7. Zones formed as a result of relative significance of nucleation and seed growth.

with decreasing CV (A and B), it can be seen that the seed growth is almost of the same order for these two points, although there is more initial seed mass and subsequent seed growth for point B than A. However, nucleation and subsequent growth of the nuclei is more pronounced for point B than A. The contribution to the value of the S_{avg} (see Table 3) is due to primary nucleation and growth. For point A, the CV is higher as the contribution to the CV (arising from the deviation of the distribution from S_{avg}) due to seed growth is more pronounced compared to that for point B. As we move from point A to B, there is more nucleation and growth of the nuclei without too much relative variation in the seed growth, resulting in higher crystal size and lower CV. Notice that higher ee for point B compared to A (see Table 3) favors more primary nucleation and subsequent growth of the nuclei.

For point C, the nucleation is much more dominant when compared to both the points A and B, and the contribution to CV due to seed growth is comparatively less significant. This leads to further decrease in CV. Notice that ee for C is closer to the maximum limit, which favors primary nucleation. For points D and E, primary nucleation is less dominant but the growth of these nuclei is more dominant and equally dominant is the seed growth. This leads to increase in the crystal size (S_{avg} still lies closer to the primary nucleation and nuclei growth region), and further reduction in CV. Notice that higher ee and slow cooling rate for both these cases favor primary nucleation as well as nuclei and seed growth. For points F and G, nucleation is least favored and seed/nuclei growth is more favored (compared to points A-E). Notice Ms is at the highest limit and ee at the lowest limit for these two points. This causes further increase in S_{avg}. The value of S_{avg} for these two cases has increasing contribution from seed growth. This causes further increase in CV where the contribution (in terms of deviation from S_{avg}) is again from both the nucleation and nuclei growth as well as seed growth. The nature of point H in Zone 3 is, however, different from that of points F and G. For point H, the nuclei growth is more pronounced when compared to seed growth. The number density distribution for point H along with point F and G is presented in Figure 9 for clarity. The difference between points F, G, and H is that for the former two points, the seed growth/initial seed size distribution is prominent while for the latter the growth of the nuclei is prominent. Notice the smaller value of Ms for point H compared to that of F and G. This causes reduced CV for point H.

Transition from point C-H is also accompanied by decreased rate of cooling. It is also responsible for higher S_{avg} from C—H. One important noticeable aspect here is that there is a maximum in productivity with respect to tf (Figure 6b). The productivity is dependant upon the relative nucleation and growth of the nuclei of the c-form compared to the combined p-form primary nucleation and growth, and the

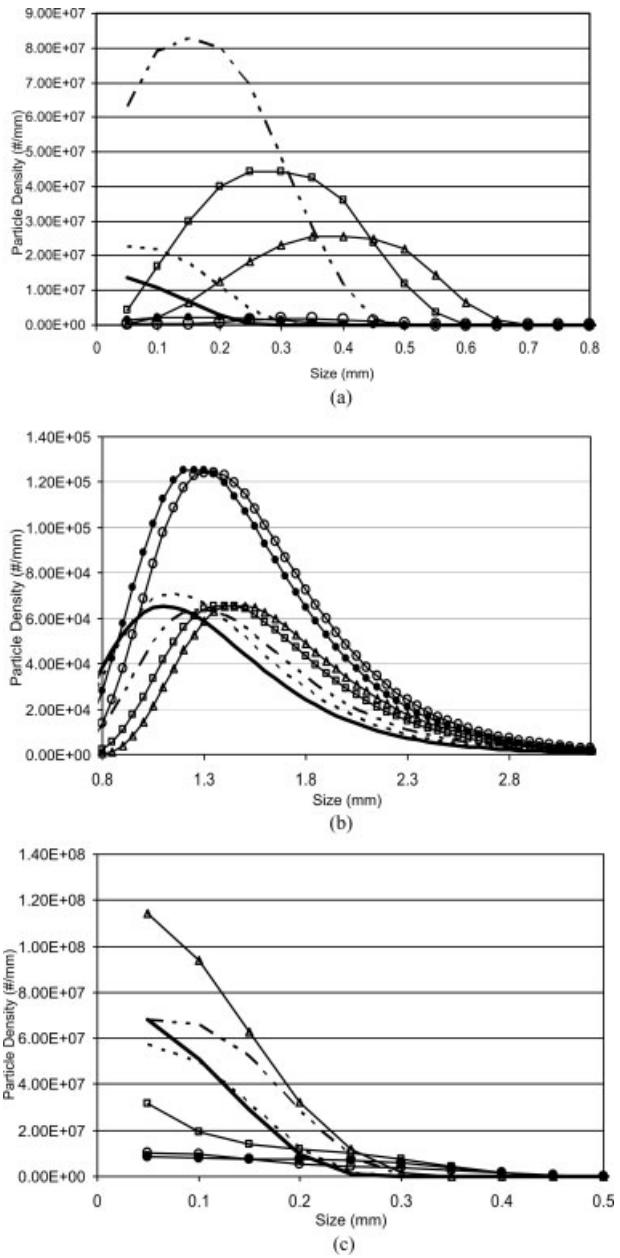

Figure 8. Particle size distribution for points A–G in Figure 7.

(a) p-form primary nucleation and growth; (b) p-form seed growth; and (c) c-form primary nucleation. ——: A; — — —: B; — — — —: C; —□—: D; —Δ—: E; —●—: F; —○—: G.

Table 3. Operating Conditions Corresponding to Points A–G in Figure 7

Points	A	B	C	D	E	F	G	H
Ms	5.1749	5.6238	5.0797	5.2335	5.2335	9.9991	9.9070	5.1908
ee	0.0014	1.4818	5.8963	5.8501	5.9998	0.0251	0.2544	0.8494
T_1	32.0001	32.0002	32.0008	33.0002	33.9934	33.9688	33.4933	33.8438
T_2	27.7940	27.7897	27.7903	30.9946	33.9933	33.8372	33.4850	33.8437
T_3	27.0769	27.7890	27.7896	30.9903	33.9933	33.8361	33.4818	33.8422
T_4	27.0270	27.7876	27.6029	30.4295	33.8848	30.6678	33.4792	33.8401
T_5	27.0220	27.7860	27.5859	27.9099	30.5828	30.6649	33.4767	33.8376
T_6	26.4274	27.7741	26.5250	26.8741	26.9873	30.5798	33.4593	33.8208
T_7	26.3931	27.0803	26.4049	26.8416	26.2100	30.0525	31.7473	33.8204
T_8	25.9285	27.0750	26.3025	26.3924	26.0314	28.3928	31.1361	33.8095
T_9	25.9038	27.0684	26.1096	26.0464	25.7028	28.3022	31.1069	33.7798
T_{10}	25.8813	27.0660	25.9273	25.8041	25.3667	27.7566	30.0472	33.7748
T_{11}	25.7375	27.0643	25.8251	25.7700	25.3071	27.3067	29.9136	33.6399
T_{12}	25.3411	27.0277	25.1873	25.5539	25.1421	25.4727	29.3105	33.5652
T_{13}	25.3171	27.0107	25.1256	25.5291	25.1318	25.4394	27.0278	33.5299
T_{14}	25.2783	26.7885	25.0282	25.0741	25.0833	25.3874	26.8038	33.0645
T_{15}	25.2436	26.6117	25.0217	25.0656	25.0729	25.3421	26.6274	32.6483
T_{16}	25.1834	26.3976	25.0131	25.0395	25.0549	25.2589	26.4022	32.0888
T_{17}	25.1074	26.0916	25.0070	25.0270	25.0278	25.2158	26.2701	31.1013
T_{18}	25.0787	25.8357	25.0059	25.0205	25.0208	25.1480	25.9671	30.1143
T_{19}	25.0609	25.6397	25.0048	25.0028	25.0161	25.0776	25.2543	27.0212
T_{20}	25.0415	25.4523	25.0035	25.0008	25.0110	25.0528	25.0220	26.4291
tf	52.3116	52.8730	55.9178	88.9279	133.7672	139.1464	215.6490	360.9486
S_{avg}	0.1254	0.1347	0.1904	0.2920	0.3791	0.3990	0.5626	0.5810
CV	1.9229	1.3466	0.6519	0.5070	0.4491	1.3612	1.0192	0.7483
Pr	0.0145	0.0067	0.0211	0.0693	0.0899	0.0471	0.0556	0.0528

seed growth. Beyond certain critical value of tf (corresponding to point P in Figure 6b), increased S_{avg} can only be obtained at the expense of reduced ee, less cooling rate and more time. These factors favor primary nucleation of c-form as well and there is drop in Pr after certain tf.

All the points in the Pareto optimal solution have, thus, been obtained through the relative significance of the primary nucleation and nuclei growth for both the p and c-forms and the seed growth of the p-form. This is caused due to the complex interplay between the rate of cooling, ee and Ms. It can be seen that there is some discontinuity while going from Zone 1 to Zone 2 and increase in the spread while transition from Zone 2 to Zone 3 (see Figure 7). The discontinuity can be regarded as the obvious manifestation of some of the facts stated in the previous paragraph. Zone 1 characterizes onset of primary nucleation and growth of the nuclei of p-form with a significant contribution to the CV from the seed growth (or initial seed size distribution). Zone 2 is associated with substantial primary nucleation, growth of the primary nuclei, and relatively less significant seed growth (or initial seed size distribution). The transition from Zone 1 to Zone 2 is thus marked by dominance from seed growth (or initial seed size distribution) to primary nucleation. Because there is a discontinuity in the size range of nucleation and initial seed distribution, the same is observed in terms of discontinuity with respect to objective functions for transition from Zone 1 to Zone 2.

The factors that facilitate nuclei formation and favor seed growth in Zone 2 will involve increase in Ms, tf and decrease in the cooling rate. This ultimately leads to operation in Zone 3. Zone 3, thus, has conditions favorable for the seed growth as well as nuclei growth (with less extent of nuclei formation) while Zone 2 has conditions more favorable for nucleation and nuclei growth. This causes more spread in the optimal solution for Zone 3 when compared to Zone 2. The transition in these three regions is, thus, accompanied by relative change in the significance of different dominating phenomena of seed growth and primary nucleation. The transition is sharp as there is discontinuity in the size range of nucleation and seed distribution, which also manifests in terms of sudden change in the characteristic (discontinuity and change in spread) in the optimum values as well.

A better analysis of the transition between these zones can be obtained by considering the solutions at different values of purity as reported in Figure 10 (for CV vs. tf plots only). It can be seen that the discontinuity for transition from Zone 1 to 2 is eliminated as purity requirements are lowered from 95 to 85% for the p-form and transition from Zone 2 to Zone 3 occurs at higher tf value. Zone 1 is characterized by increasing nucleation and nuclei growth of p-form and decreasing CV caused due to the decreased contribution of seed growth/initial seed distribution. A smoother transition from Zone 1 to 2 will require more nucleation of p-form which can not be achieved without more nucleation of c-form. Therefore, a continuous transition is obtained at lower values of purity that facilitates more nucleation for c-form. Reduced purity requirements also extend the region of primary nucleation and nuclei growth dominant Zone 2 as conditions favorable to nucleation and nuclei growth for p-form are generated along with the favorable nucleation and nuclei growth of c-form. It must be mentioned that the moment based model used in this work is able to distinguish between the nucleation dominated and the seed growth dominated

regions. The qualitative picture obtained using moment based model can be further refined in the region of interest using the detailed population balance model. However, the moment based model will always be preferred for online optimizing control.

The multi-objective optimization framework is, thus, able to explore various regimes of importance in preferential crystallization both qualitatively as well as quantitatively. The main observations and conclusions from this study are summarized below.

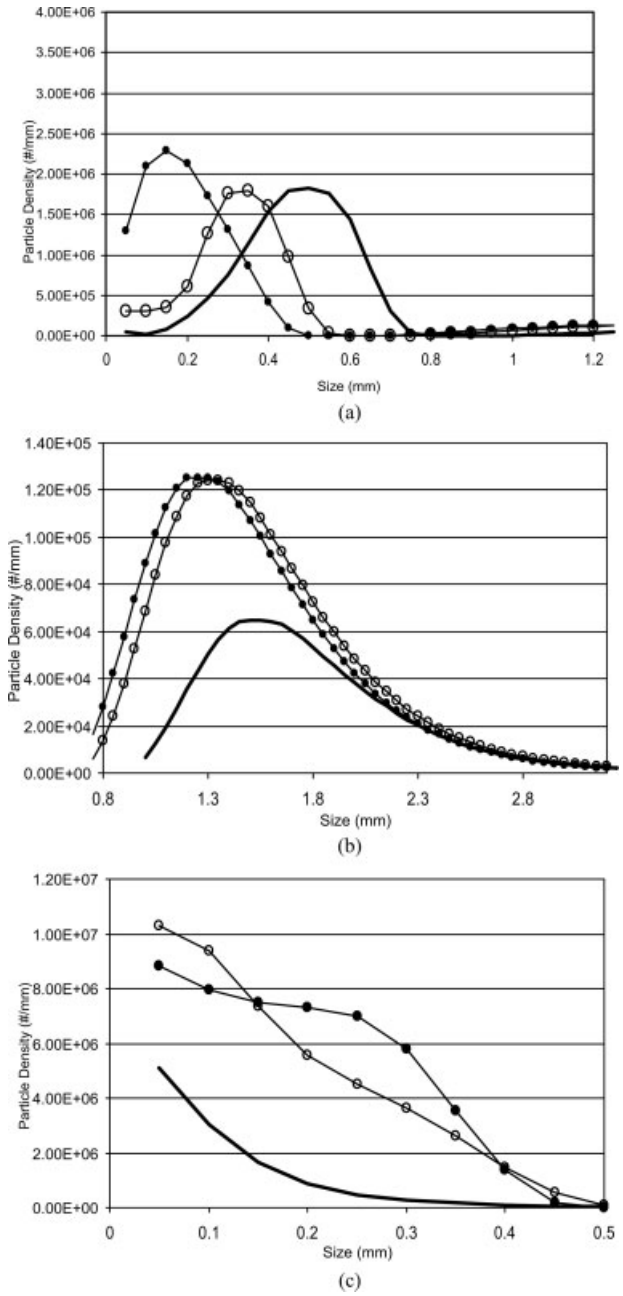

Figure 9. Particle size distribution for points F–H in Figure 7.

(a) p-form primary nucleation and growth; (b) p-form seed growth; and (c) c-form primary nucleation. —●—: F; —⊖—: G; ——: H.

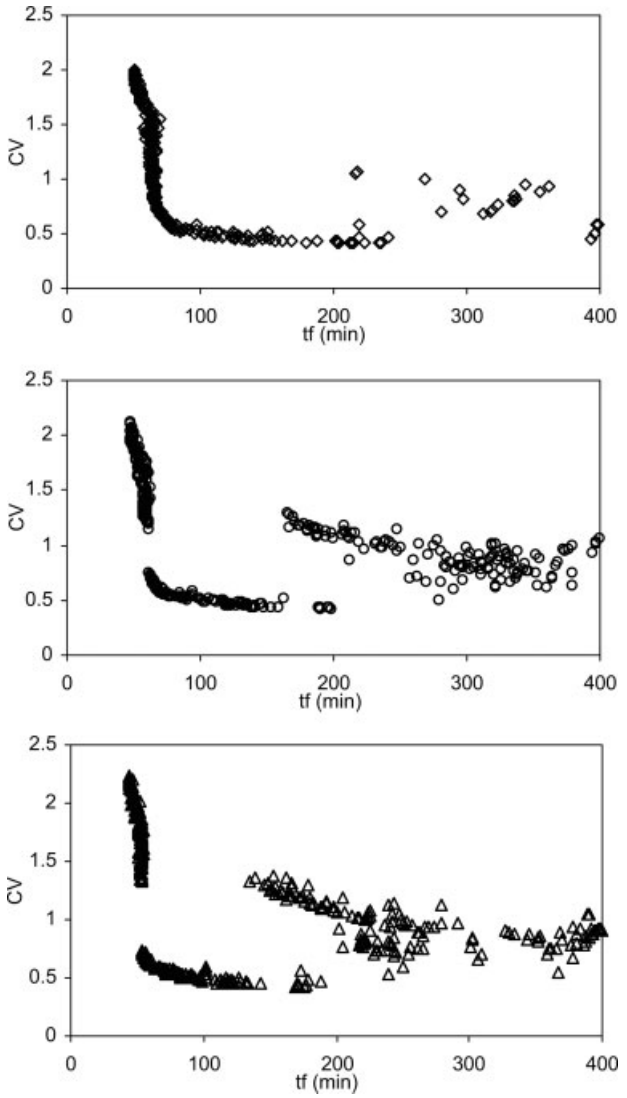

Figure 10. Pareto optimal solution for different purity values. ◇: Pu = 85%; ○: Pu = 90%; △: Pu = 95%.

Conclusions

Some of the important conclusions from this analysis are as follows. These conclusions are specific to the example discussed in this study. However, these can be considered generic as their qualitative basis is derived from the relative significance of various mechanisms involved in preferential crystallization.

For a given desired purity of the p-form,

(1) There is a maximum in productivity that can be attained for the given system, which also corresponds to minimum CV.

(2) A small increase in time (in the time range 50–55 min) helps in reducing the CV substantially. This region is, however, dominated by pronounced primary nucleation and growth.

(3) Zone 3 is important for exploring more seed growth and less primary nucleation. This region is marked by higher tf values and reduced yield.

The analysis reported in this study gives the overall picture and helps the decision maker in arriving at the correct configuration based on his/her requirement and the operating constraints. Detailed analysis in the specific region of interest can be carried out using higher resolution models for better precision. The focus of this work is to highlight various regimes that are obtained through interplay between nucleation and growth associated with the crystallization. The qualitative analysis will remain the same under different operating conditions. The solutions obtained can be further improved in terms of spread in all the zones and convergence time using suitable adaptations of the genetic algorithm and the further efforts constitute our future work.

We would like to emphasize that the main thrust of this study is to theoretically address the multiobjective aspect of the preferential crystallization using available information in the literature. To the best of our knowledge, this has been attempted for the first time for preferential crystallization. The study presented here is generic, and the values of various parameters are chosen based on the existing values available in the literature. However, this study can be extended for problems involving other combinations of objectives, constraints, and decision variables as suited to the industry.

Literature Cited

1. Collins AN, Sheldrake GN, Crosby J. *Chirality in Industry. II. The Commercial Manufacture and Applications of Optically Active Compounds*. New York: Wiley, 1997.
2. Rouhi AM. Chirality at work. *Chem Eng News*. 2003;81:56–61.
3. Schulte M, Strube J. Preparative enantioseparation by simulated moving bed chromatography. *J Chromatogr A*. 2001;906:399–416.
4. Juza M, Mazzotti M, Morbidelli M. Simulated moving-bed chromatography and its application to chirotechnology. *Trends Biotechnol*. 2000;18:108–118.
5. Angelov I, Raisch J, Elsner MP, Seidel-Morgenstern A. Optimal operation of enantioseparation by batch-wise preferential crystallization. *Chem Eng Sci*. 2008;6:1586–1601.
6. Elsner MP, Ziomek G, Seidel-Morgenstern A. Simultaneous preferential crystallization in a coupled, batch operation mode—Part I: theoretical analysis and optimization. *Chem Eng Sci*. 2007;62:4760–4769.
7. Lorenz H, Perlberg A, Sapoundjiev D, Elsner MP, Seidel-Morgenstern A. Crystallization of enantiomers. *Chem Eng Process*. 2006;45: 863–873.
8. Qamar S, Ashfaq A, Angelov I, Elsner MP, Warnecke G, Seidel-Morgenstern A. Numerical solutions of population balance models in preferential crystallization. *Chem Eng Sci*. 2008;5:1342–1352.
9. Qamar S, Ashfaq A, Warnecke G, Angelov I, Elsner MP, Seidel-Morgenstern A. Adaptive high-resolution schemes for multidimensional population balances in crystallization processes. *Comput Chem Eng*. 2007;31:1296–1311.
10. Qamar S, Elsner MP, Angelov IA, Warnecke G, Seidel-Morgenstern A. A comparative study of high resolution schemes for solving population balances in crystallization. *Comput Chem Eng*. 2006;30: 1119–1131.
11. Rohani S, Bourne JR. A simplified approach to the operation of a batch crystallizer. *Can J Chem Eng*. 1990;68:795–806.
12. Miller SM, Rawlings JB. Model identification and control strategies for batch cooling crystallizers. *AIChE J*. 1994;40:1312–1327.
13. Lang Y, Cervantes AM, Biegler LT. Dynamic optimization of a batch cooling crystallization process. *Ind Eng Chem Res*. 1999;38: 1469–1477.
14. Costa CBB, Filho RM. Evaluation of optimisation techniques and control variable formulations for a batch cooling crystallization process. *Chem Eng Sci*. 2005;60:5312–5322.
15. Hu Q, Rohani S, Jutan A. Modeling and optimization of batch seeded cooling crystallizers. *Comput Chem Eng*. 2005;29:911–918.
16. Chung SH, Ma DL, Braatz RD. Optimal seeding in batch crystallization. *Can J Chem Eng*. 1999;77:590–596.
17. Choong KL, Smith R. Novel strategies for optimization of batch, semi-batch and heating/cooling evaporative crystallization. *Chem Eng Sci*. 2004;59:329–343.
18. Vollmer U, Raisch J. Control of batch cooling crystallization processes based on orbital flatness. *Int J Control*. 2003;76:1635–1643.
19. Feng L, Berglund KA. ATR-FTIR for determining optimal cooling curves for batch crystallization of succinic acid. *Cryst Growth Des*. 2002;2:449–452.
20. Hojjati H, Rohani S. Cooling and seeding effect on supersaturation and final crystal size distribution (CSD) of ammonium sulphate in a batch crystallizer. *Chem Eng Process*. 2005;44:949–957.
21. Kubota N, Doki N, Yokota M, Sato A. Seeding policy in cooling crystallization. *Powder Technol*. 2001;121:31–38.
22. Ge M, Wang QG, Chiu MS, Lee TH, Hang CC, Teo KH. An effective technique for batch process optimization with application to crystallization. *Chem Eng Res Des*. 2000;78:99–106.
23. Zhang G, Rohani S. On-line optimal control of a seeded batch crystallizer. *Chem Eng Sci*. 2003;58:1887–1896.
24. Goldberg DE. *Genetic Algorithms in Search, Optimization and Machine Learning*. Addison-Wesley: Reading, MA, 1989.
25. Deb K, Pratap A, Agarwal S, Meyarivan T. A fast and elitist multiobjective genetic algorithm: NSGA-II. *IEEE Trans Evol Comput*. 2002;6:182–197.
26. Bhaskar V, Gupta SK, Ray AK. Multiobjective optimization of an industrial wiped film poly(ethylene terephthalate) reactor. *AIChE J*. 2000;46:1046–1058.
27. Kasat RB, Gupta SK. Multiobjective optimization of an industrial fluidized-bed catalytic cracking unit (FCCU) using genetic algorithm with the jumping genes operator. *Comput Chem Eng*. 2003;27:1785–1800.
28. Guria C, Bhattacharya PK, Gupta SK. Multiobjective optimization of reverse osmosis desalination units using different adaptations of the nondominated sorting genetic algorithm (NSGA). *Comput Chem Eng*. 2005;29:1977–1995.
29. Agarwal A, Gupta SK. Multi-objective optimal design of heat exchanger networks using new adaptations of the elitist non-dominated sorting genetic algorithm, NSGA-II. *Ind Eng Chem Res*. 2008;47:3489–3501.
30. Sarkar D, Rohani S, Jutan A. Multi-objective optimization of seeded batch crystallization processes. *Chem Eng Sci*. 2006;61:5282–5295.
31. Amanullah A, Mazzotti M. Optimization of a hybrid chromatography-crystallization process for the seperation of Troger's base enantiomers. *J Chromatogr A*. 2006;1107:36–45.
32. Angelov I, Raisch J, Elsner MP, Seidel-Morgenstern A. Optimal operation of enantioseparation by batch-wise preferential crystallization. *Chem Eng Sci*. 2008;63:1282–1292.
33. Elsner MP, Menendez DF, Muslera EA, Seidel-Morgenstern A. Experimental study and simplified mathematical description of preferential crystallization. *Chirality*. 2005;17:S183–S195.
34. Ramkrishna D. *Population Balances: Theory and Applications to Particulate Systems in Engineering*. San Diego, CA: Academic Press, A Harcourt Science and Technology Company, 2000.
35. Shi D, Mhaskar P, El-Farra NH, Christofides PD. Predictive control of crystal size distribution in protein crystallization. *Nanotechnology*. 2005;16:S562–S574.
36. Mersmann A. *Crystallization Technology Handbook*. New York: Marcel Dekker, 2001.
37. Randolph AD, Larson MA. *Theory of Particulate Processes. Analysis and Techniques of Continuous Crystallization*. San Diego, CA. Academic Press, 1998.
38. Qamar S, Ashfaq A, Angelov I, Elsner MP, Warnecke G, Seidel-Morgenstern A. Numerical solutions of population balance models in preferential crystallization. *Chem Eng Sci*. 2008;63:1342–1352.
39. Traub JF. On Lagrange-Hermite interpolation. *J Soc Ind Appl Math*. 1964;12:886.
40. Bhat SA, Saraf DN, Gupta S, Gupta SK. On-line optimizing control of bulk free radical polymerization reactors under temporary loss of temperature regulation: experimental study on a 1-L batch reactor. *Ind Eng Chem Res*. 2006;45:7530–7539.

Manuscript received Mar. 31, 2008, and revision received Aug. 21, 2008.